The role of glycine in the iron-phosphorous alloy electrodeposition

Natalia Kovalska [a, b, *], Martin Pfaffeneder-Kmen [a], Natalia Tsyntsaru [c], Rudolf Mann [b], Henrikas Cesiulis [c], Wolfgang Hansal [b], Wolfgang Kautek [a, *]

[a] University of Vienna, Department of Physical Chemistry, A-1090 Vienna, Austria
[b] Hirtenberger Engineered Surfaces GmbH, A-2552 Hirtenberg, Austria
[c] Vilnius University, Department of Physical Chemistry, LT-03225 Vilnius, Lithuania

A B S T R A C T

The influence of glycine on the iron phosphorous alloy electrodeposition was investigated by electrochemical quartz microbalance (EQMB), *in-situ* external reflection FTIR spectroscopy, and electrochemical impedance spectroscopy (EIS) measurements. An increase of glycine concentration leads to a decrease of the iron-phosphorous alloy electrodeposition rate and an increase of hydrogen evolution. Strong adsorption of glycine species, such as $H_2(gly)^+$, $H(gly)^{\pm}$ or/and $Fe(gly)^+$, have been observed during the hydrogen evolution and the Fe-P deposition reaction. Due to the concurrent hydrogen evolution the pH attains higher values at the interface than in the electrolyte bulk (pH2.5). The formation of adsorbed $Fe(gly)^+$ and of the chelate complex $Fe(gly)_2$ in solution avoids the precipitation of $Fe(OH)_2$ in the pH range between 2.5 and ca. 7 at the interface. The phosphorous content of the iron phosphorous alloy deposit increases with the glycine concentration. This is due to a lower deposition rate of iron caused by the adsorption of $Fe(gly)^+$, while the hypophosphite reduction rate to phosphorous increases.

1. Introduction

The addition of additives to electrochemical baths can strongly influence the electrodeposition of metal alloy coatings. Additives may modify the deposition mechanism, the morphology, microstructure, and physicochemical properties of the alloys. Recently, there has been enhanced interest in glycine as additive [1–5], such as in the plating of Fe [6], and of Ni-Mn alloys where the influence surface morphology and grain size was reported [7]. In the later system, the minimization of the grain size is important for nanocrystalline soft magnetic materials as well as for the increase of the corrosion resistance.

Glycine is a bidentate ligand that can coordinate via its amino and carboxyl groups forming homonuclear, binuclear and heteronuclear complexes with metal ions. A study of the formation of Fe ion complexes showed that the cationic form of glycine $(NH_3CH_2COOH)^+$ is present together with the zwitterion $(NH_3CH_2COO)^{\pm}$ for pH < 4.0. At pH > 4.0, it exists as the zwitterion, and at pH > 9.0, as the anion $(NH_2CH_2COO)^-$ [1].

The Fe-P coatings become interesting in metallic foam and battery anode deposition [8–10], in magnetic [11–14] and corrosion inhibition applications [15–17]. Moreover, high strength, hardness, relatively high electrical resistivity, and advantageous mechanical properties may be achieved [10].

Glycine is known as a buffer in order to stabilize baths (e.g. avoid $Fe(OH)_x$ precipitation) due to its zwitterion form in the pH range of ca. 5–8 (pK_{a1} = 2.3, pK_{a2} = 9.6) [18,19]. It can also promote hydrogen evolution and thus lead to an increase of the phosphorous content in the coatings [20]. The formation and participation of Fe hydroxide species due to the pH increase caused by the concurrent hydrogen evolution during the Fe-Mo-P electrodeposition was repeatedly investigated.

The behaviour of glycine on gold electrodes was studied by in-situ IR spectroscopy [4,5,21]. It was shown that, during cobalt electrodeposition, the pH has a drastic influence on the glycine deprotonation and the formation of Co glycine complexes [4,5,21].

The detailed mechanism of Fe-P electrodeposition has received limited attention. In the present study, a mechanistic investigation of the influence of glycine on the Fe-P electrodeposition is presented applying *in-situ* techniques such as the Electrochemical Quartz Microbalance (EQMB), *in-situ* external reflection FTIR spectroscopy, and Electrochemical Impedance Spectroscopy (EIS).

2. Experimental

The electrolyte for the Fe-P electrodeposition consisted of 0.7 M $FeSO_4 \cdot 7H_2O$, 0.06 M $NaH_2PO_2 \cdot H_2O$, and $NH_2CH_2CO_2H$ (glycine). The concentration of glycine was varied (0.10, 0.21, 0.32, 0.43, 0.64 M) in order to investigate the influence of glycine on the deposition mechanism. Analytical grade chemicals and deionized water were used. The working pH range was chosen from 1 to 3 in order to prevent too strong hydrogen evolution or precipitation of $Fe(OH)_2$. It was optimized at 2.5 by the addition of sulphuric acid. All measurements were carried out at room temperature.

Thermodynamic calculations for the chemical speciation diagrams were performed by a software (Medusa-Hydra chemical equilibrium software).

The Electrochemical Quartz Microbalance (EQMB) measurements were performed with a dedicated three-electrode cell with QMB working electrode (potentiostat: Autolab, PGSTAT equipped with an EQCM module). The gold surface was cleaned by cycling in 0.1 M H_2SO_4 solution. Frequency measurements were performed with a 6 MHz, AT-cut quartz crystal coated with a 100 nm thick gold layer (exposed area 0.384 cm^2). A gold coil was used as a counter electrode and an Ag/AgCl/3 M KCl electrode as reference electrode (+0.21 V vs. standard hydrogen electrode, SHE) [22]. For better data evaluation, the potentials (U) are presented versus the SHE.

In-situ external reflection FTIR spectroscopy was performed with a FTIR spectrometer (Bruker Vertex 70). An external liquid-nitrogen cooled LN-MCT detector was employed. The beam delivery optics was positioned on an aluminium breadboard in a CO_2- and water-free air-flushed compartment. A conventional three-electrode setup (potentiostat: Electrochemical Workstation, CH-Instruments 760C) with a platinum wire as counter electrode and an Ag/AgCl/3 M KCl electrode as reference electrode (+0.21 V vs. SHE) were used. The working electrode was mounted on a glass tube precisely positioned relative to the ZnSe window by a micrometer head with a resolution of 1 μm [23]. The spectra were measured under p-polarization. The sampling time for each spec-trum was 25 s.

EIS measurements were carried out in a three-electrode cell (0.3 L) without stirring using an impedance spectroscopy setup (Autolab, PGSTAT302 N combined with a FRA32 M module; Vilnius University). Brass (1 cm^2) was used as a non-costly working electrode because only cathodic potentials were applied. Brass plates with a surface area of 2.25 cm^2 were used as working electrodes for the galvanostatic electrodeposion of Fe-P coatings. It was ultrasonically cleaned in 0.1 M sulphuric acid (5 min) before measurements. The reference electrode was Ag/AgCl 3 M KCl, (+0.21 V vs. SHE).

The surfaces were characterised with a scanning electron microscope (Hitachi FEG-SEM S4800) and with EDX for elemental analysis.

3. Results and discussion

3.1. Fe-P glycine solution equilibria

Glycine, NH_2-CH_2-COOH or H(gly), is an amino acid and can exist as a zwitterion, NH_3^+-CH_2-COO^- or $H(gly)^{\pm}$, subject to the following chemical equilibria (with logarithms of the stability constants (log K, ionic strength 1.0) in the iron-glycine system (data from Ref. [24]):

$$H(gly)^{\pm} + H^+ \rightleftharpoons H_2(gly)^+ \ (\log K = 12.1) \quad (1)$$

$$H(gly)^{\pm} \rightleftharpoons H^+ + (gly)^- \ (\log K = 9.7). \quad (2)$$

Eq. (1) corresponds to the carboxyl group protonation of the zwitterion $H(gly)^{\pm}$ resulting in NH_3^+-CH_2-$COOH^-$ or $H_2(gly)^+$, and Eq. (2) corresponds to the amino group deprotonation leading to NH_2-CH_2-COO^- or $(gly)^-$. This glycinate ion, $(gly)^-$, is able to form five-member chelate rings with Fe^{2+} ions. Three complex species formed with Fe^{2+} predominate in solution depending on pH:

$$Fe^{2+} + (gly)^- \rightleftharpoons Fe(gly)^+ \ (\log K = 4.31) \quad (3)$$

$$Fe(gly)^+ + (gly)^- \rightleftharpoons Fe(gly)_2 \ (\log K = 8.32) \quad (4)$$

$$Fe(gly)_2 + (gly)^- \rightleftharpoons Fe(gly)_3^- \ (\log K = 9.79). \quad (5)$$

The increase of pH promotes the iron glycinate coordination, as seen in the chemical species distribution (Fig. 1). These calculated results suggest the existence of iron glycinate complexes only beyond pH 4. This is greater than the pH of 2.5 chosen in all presented experiments. However, it has to be considered that hydrogen evolution parallel to the metal deposition will increase the pH so that all the mentioned Fe glycinate complex species may play a role (Fig. 1a). Interestingly, the calculations suggest a dominance of Fe hydroxide species over the glycinates at elevated pH. That may compete with the interfacial role of the glycine species stable at pH 2.5, which are $H_2(gly)^+$ and H(gly).

Considering the complexing activity of sulphate species besides glycinate one has to consider the formation of a solvated $[FeHSO_4]^+_{aq}$ associate at pH values less than 3 (Fig. 1b) which range is irrelevant in the present experiments:

$$Fe^{2+} + H^+ + SO_4^{2-} \rightleftharpoons [FeHSO_4]^+_{aq} \ (\log K = 3.07). \quad (6)$$

At moderate acidity, the formation of the ion pair $[FeSO_4]_{aq}$ can be calculated (Fig. 1b):

$$Fe^{2+} + SO_4^{2-} \rightleftharpoons [FeSO_4]_{aq} \ (\log K = 2.25). \quad (7)$$

A further increase in pH leads to the formation of iron hydroxo-complexes [25]:

$$Fe^{2+} + H_2O \leftrightarrow [FeOH]^+_{aq} + H^+ \ (\log K = -7.93) \quad (8)$$

$$Fe^{2+} + 2H_2O \leftrightarrow [Fe(OH)_2]_s + H^+ \ (\log K = -18.94). \quad (9)$$

$[FeOH]^+_{aq}$ can only be formed to a significant extent when glycinate is absent (Eq. (8)).

3.2. Potentiodynamic investigations

The characterization of the cathodic reduction reaction of Fe^{2+} in the Fe-P electrolyte was investigated by cyclic voltammograms (CV) in combination with electrochemical quartz crystal microbalance (EQMB) measurements. Fig. 2 shows the voltammetric response in the Fe-P electrolyte containing 0.21 M glycine at pH 2.5. The cathodic reversal potential, U_c, was varied. The potential scans started at the respective OCP (open circuit potential) around +0.3 V in negative direction. Two cathodic waves were observed which will be discussed based on data in Fig. 3. The anodic current peaks correspond to the oxidative stripping of Fe-P electrodeposited at $U < -0.74$ V where Fe-P formation begins. Actually, a reversal potential U_c of −0.74 V up to ca. −0.3 V resulted in no Fe-P deposition and, therefore, no anodic stripping peak.

Measured frequency changes, Δf, were related to interfacial mass changes by the Sauerbrey equation:

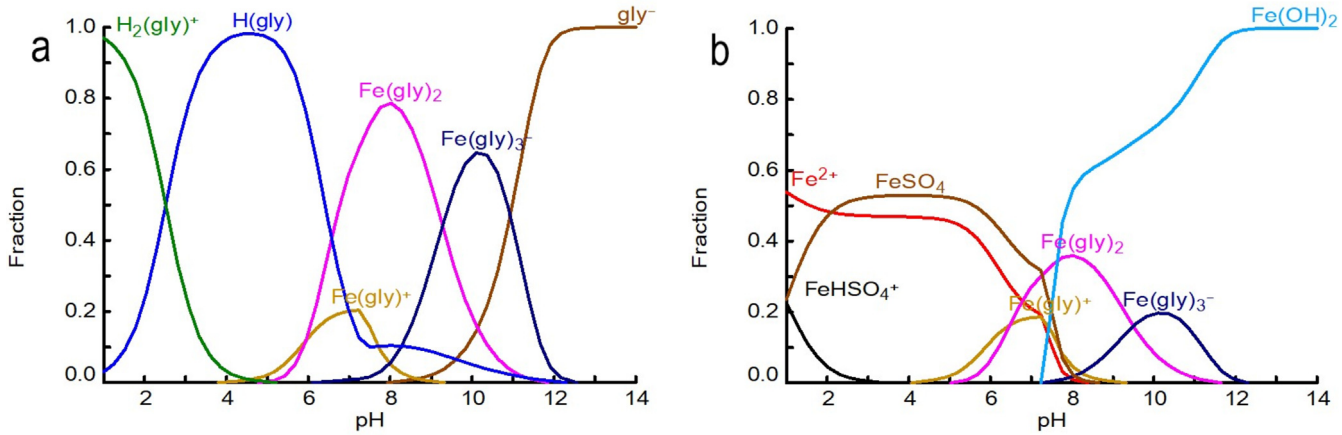

Fig. 1. Species distribution vs. pH. (a) glycine species; (b) Fe^{2+} species. Fe-P glycine electrolyte: 0.7 M $FeSO_4$; 0.06 M $NaH_2PO_2 \cdot H_2O$; 0.6 M glycine.

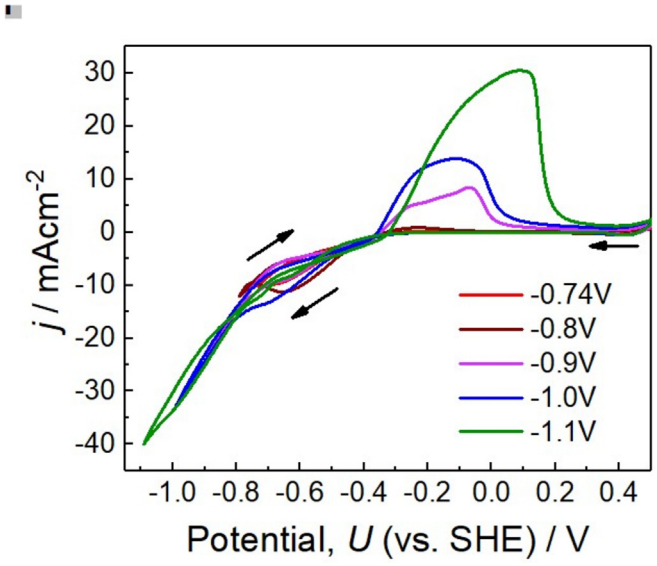

Fig. 2. Cyclic voltammograms of Fe-P glycine electrolyte with varying cathodic reversal potential U_c (inserted) at constant anodic reversal potential, $U_a = +0.5$ V. 0.7 M $FeSO_4$; 0.06 M $NaH_2PO_2 \cdot H_2O$; 0.21 M glycine.

$$\Delta f = -\frac{2f_0^2}{A\sqrt{\rho_q \mu_q}}\Delta m \tag{10}$$

where f_0 is the nominal resonant frequency of the crystal, Δm is the mass change, A is the area of the gold electrode exposed to the electrolyte, ρ_q is the density of quartz and μ_q is the shear modulus of quartz. Eq. (10) can be reduced to

$$\Delta f = -C_f \Delta m \tag{11}$$

where is C_f is the sensitivity coefficient of the quartz crystal balance ($C_f = 0.0815$ Hz/ng/cm^2 for a 6 MHz crystal).

The EQMB measurement allowed to quantify the charge and mass of the electrodeposition of the Fe-P phase and the total charge of the hydrogen evolution on the bare and Fe-P-covered gold electrode (Fig. 3). Hydrogen evolution on naked gold sets in at $U < -0.40$ V indicated by a negative current wave, a charge increase, q^-_H(Au), and constant frequency/mass (vertical dashed line at H^+/H_2). At $U \approx -0.75$ V (vertical dashed line at Fe^{2+}/Fe) a frequency change indicates a mass increase due to Fe-P deposition both for the negative and the positive scan. The measured charge change however, is correlated to both this deposition reaction and the hydrogen evolution on the Fe-P surface, $q^-_{H/Fe\text{-}P}$(Fe-P). On the reverse scan, at ca. −0.75 V, the deposition stops indicated by a constant frequency trace, while hydrogen still is evolved represented by a charge increase, q^-_H(Fe-P). The further anodic scan shows the stripping of most of the Fe-P phase by an anodic charge change, $q^-_{Fe\text{-}P}$, and a frequency increase. The charge difference at potentials more positive than about +0.1 V, q^{tot}_H, represents the hydrogen evolution charge on both bare gold and the Fe-P surface because the Fe-P layer has been stripped after the anodic potential scan.

The charge of the hydrogen evolution during the deposition on Fe-P layer, q^-_H(Fe-P), is:

$$q^-_H(\text{Fe-P}) = q^{tot}_H - q^-_H(\text{Au}). \tag{12}$$

The extent of the Fe-P deposition given by the frequency change, $\Delta f_{Fe\text{-}P}$, corresponding to a respective mass change (comp. Fig. 3), and the anodic stripping charge density of the Fe-P deposit, $\Delta q^-_{Fe\text{-}P}$ (comp. Fig. 3), decreases strongly with the glycine concentration (Fig. 4). This coincides with an increase of the hydrogen evolution on bare gold and on the Fe-P film, i.e. Δq^-_H(Au) and Δq^-_H(Fe-P). That means that the current efficiency of the Fe-P deposition drops with the glycine concentration [26].

The hydrogen evolution charge density, Δq^-_H(Au) and Δq^-_H(Fe-P), increases with the glycine concentration because various species act as proton donors so that the pH value in immediate proximity to the electrode surface attains pH values higher than 2.5. Starting out with a pH 2.5, the concentration of the totally protonated entity, $H_2(gly)^+$, and the zwitterion, $H(gly)^\pm$, is about equal (Fig. 1). Both these species, $H_2(gly)^+$ and the $H(gly)^\pm$, can accelerate the hydrogen evolution rate due to their deprotonation at increasing pH [4,27]. It should be mentioned that the dependence Δq^-_H(Fe-P) on the glycine concentration is higher than that of Δq^-_H(Au). This may be correlated to the higher catalytic activity of the Fe-P substrate.

The lowering of the Fe-P deposition rate can be correlated with the above described steady state of high pH near the surface due to the vigorous proton reduction. In this situation, the proton of $H(gly)^\pm$ is exchanged by an Fe^{2+} ion forming a complex $Fe(gly)^+$ (Fig. 1), which exhibits a much lower iron reduction/deposition rate according to

$$Fe(gly)^+ + 2e^- \rightleftharpoons Fe + (gly)^- \tag{13}$$

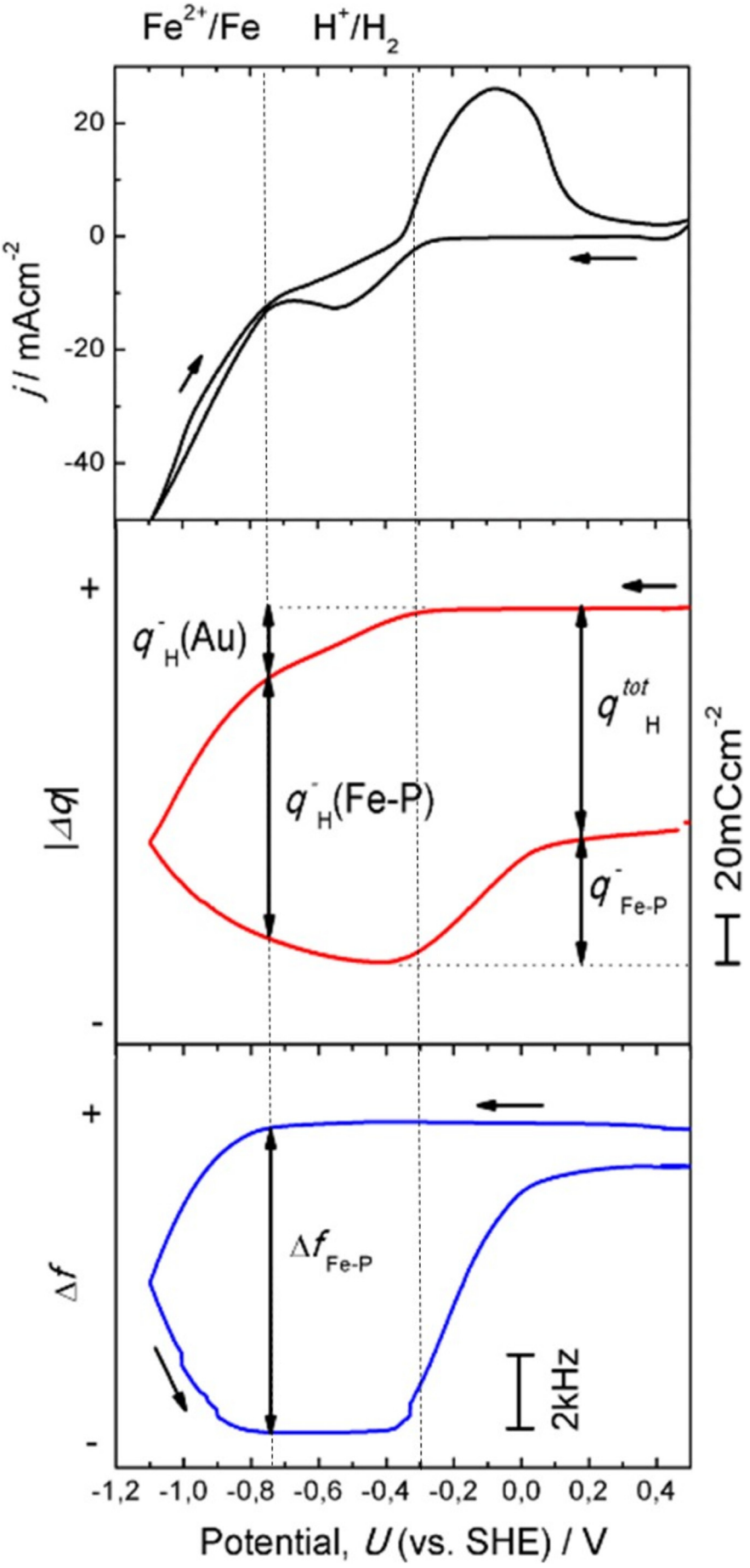

Fig. 3. Electrochemical quartz microbalance data of the Fe-P deposition (third potential cycle). 0.7 M $FeSO_4$; 0.06 M $NaH_2PO_2 \cdot H_2O$; 0.21 M glycine.

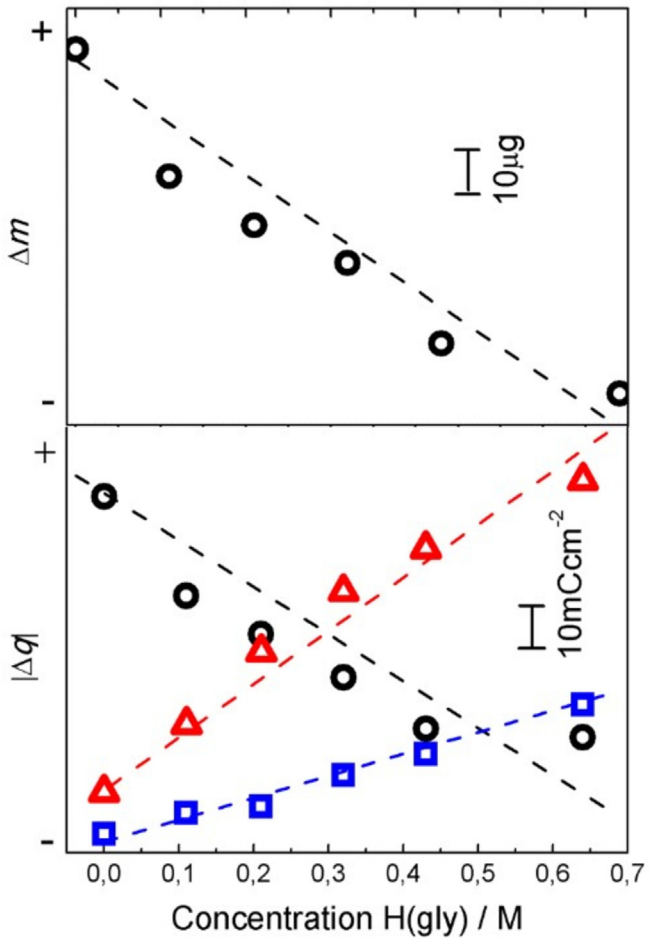

Fig. 4. Influence of the glycine concentration on the Fe-P deposition. 0.7 M $FeSO_4$; 0.06 M $NaH_2PO_2 \cdot H_2O$; 0.21 M glycine. Mass change Δm and charge density change Δq^- from electrochemical quartz microbalance evaluations (third potential cycle). Fe-P deposition given by Δm and $\Delta q^-_{Fe\text{-}P}$. Hydrogen evolution on Au, Δq^-_H (Au): □. Hydrogen evolution on Fe-P Δq^-_H(Fe-P): △.

than the hydrated Fe^{2+} ion at low pH [28]:

$$Fe^{2+} + 2e^- \rightleftharpoons Fe \ (U^\circ = -0.44\,V). \quad (14)$$

The possibility of the formation of $Fe(OH)_2$ (Fig. 1) may lead to precipitates $[Fe(OH)_2]_s$ at higher pH >3. This could be reduced according to Ref. [28]:

$$[Fe(OH)_2]_s + 2\,e^- \rightleftharpoons Fe + 2\,OH^- \ (U^\circ = -0.89\,V). \quad (15)$$

The ion pair $[FeOH]^+$ does not occur in the presence of glycine according to the calculations in Fig. 1b. Therefore, its reduction is improbable [28]:

$$[FeOH]^+ + H^+ + 2\,e^- \rightleftharpoons Fe + H_2O \ (U^\circ = -0.16\,V). \quad (16)$$

3.3. In-situ FTIR measurements

The electrode interface was investigated at various electrode potentials by *in-situ* FTIR spectroscopy in the present study. Previous *in-situ* FTIR spectroscopy investigations have demonstrated that glycine adsorbs on gold at $U > 0.4$ V in perchlorate by ATR [21] and in phosphate media by both ATR and external reflection [29]. This potential range is positive of the point of zero charge (*pzc*) a t about +0.15 V [30]. The range negative of the *pzc* was studied with a cobalt glycine electrolyte by external reflection, where the electrode directly was in mechanical contact with the IR-transparent window [4]. Therefore, electrolytes were trapped in between resulting diffusion decoupling within the experimental timescale [31] always resulting in widely uncontrollable ionic concentrations.

This beforementioned procedure is in contrast to the presently applied technique with a controllable gap between window and electrode [23]. *In-situ* FTIR absorption spectra of an Fe-P glycine electrolyte recorded from −0.13 V to −0.83 V at pH 2.5 are shown in (Fig. 5). An intensive broad band between 3200 cm^{-1} and 2900 cm^{-1} corresponds to C-H and NH_2 stretching modes of the glycine species. When the applied potential is $U < -0.4$ V, this positive band increases reflecting the adsorption of glycine. A weak shoulder in the O-H stretch vibration region between 3600 cm^{-1} and 3400 cm^{-1} increase with more negative potentials either.

The bands at 1500, 1446, 1412, 1331 cm^{-1} and also at 1602 cm^{-1} (Table 1, Fig. 6) are correlated with the chemical functions of glycine. Their increase at $U < -0.4$ V indicates the adsorption of glycine species in the hydrogen evolution region. Once the deposition Fe-P sets in around −0.7 V, these signals show a lower slope indicating a lower potential dependence of the glycine adsorption. These findings suggest that glycine species such as $H_2(gly)^+$ or $Fe(gly)^+$ are adsorbed during the iron phosphorous alloy deposition process.

The band around 1100 cm^{-1} may correlate with sulphate as negative going peak [4], or/and with adsorbed phosphate [29](Fig. 6). The band around 1645 cm^{-1} corresponds to water infrared absorption (δH_2O) exhibits a decrease when shifting the potential from the *pzc* towards ca. −0.3 V. This may be correlated to the exchange of solvated SO_4^{2-} anions by solvated Fe^{2+} ions. Thus, the amount of water molecules decreases because Fe^{2+} ions can accommodate less solvation molecules (ionic radius 0.210 nm) than the larger SO_4^{2-} anions (ionic radius 0.381 nm) [32]. Once protons are reduced and glycine adsorbed at $U < -0.7$ V, an increased band around 1645 cm^{-1} suggests the accumulation of water solvent molecules at the surface. The depletion of H_2gly^+ as a consequence of the hydrogen evolution reaction may be evidenced by the negative band at 1740 cm^{-1} which can be related to ν C=O stretching and ν COH bending, i.e., the vibrational modes of protonated carboxyl [4,33].

Bare gold is a poor catalytic surface for the hydrogen evolution from a water-solvated proton which can be thermodynamically be expected negative of $U \sim -0.16$ V (pH 2.5). This reaction only occurs at $U < -0.30$ V where glycine adsorption occurs. This suggests that the protonated glycine species $H_2(gly)^+_{ads}$ adsorbed at the negatively charged electrode surface provides a catalytically advantageous surface species. This complex can be reduced according to

$$2H_2(gly)^+ + e^- \rightleftharpoons H_2 + 2(gly)^-. \quad (17)$$

3.4. Electrochemical impedance spectroscopy measurements

Electrochemical impedance spectroscopy was performed as a function of potential in the range from −0.4 V where hydrogen evolution and glycine adsorption started and −0.8 V where Fe-P electrodeposition was just initiated (i.e. −0.75 V, comp. Fig. 3). The Nyquist plot in the absence of glycine (Fig. 7) exhibits an intricate mechanism. Even the electrodeposition of pure iron from a sulphate solutions involves at least six intermediate stages comprising three stages with adsorbed species [34]. In the absence

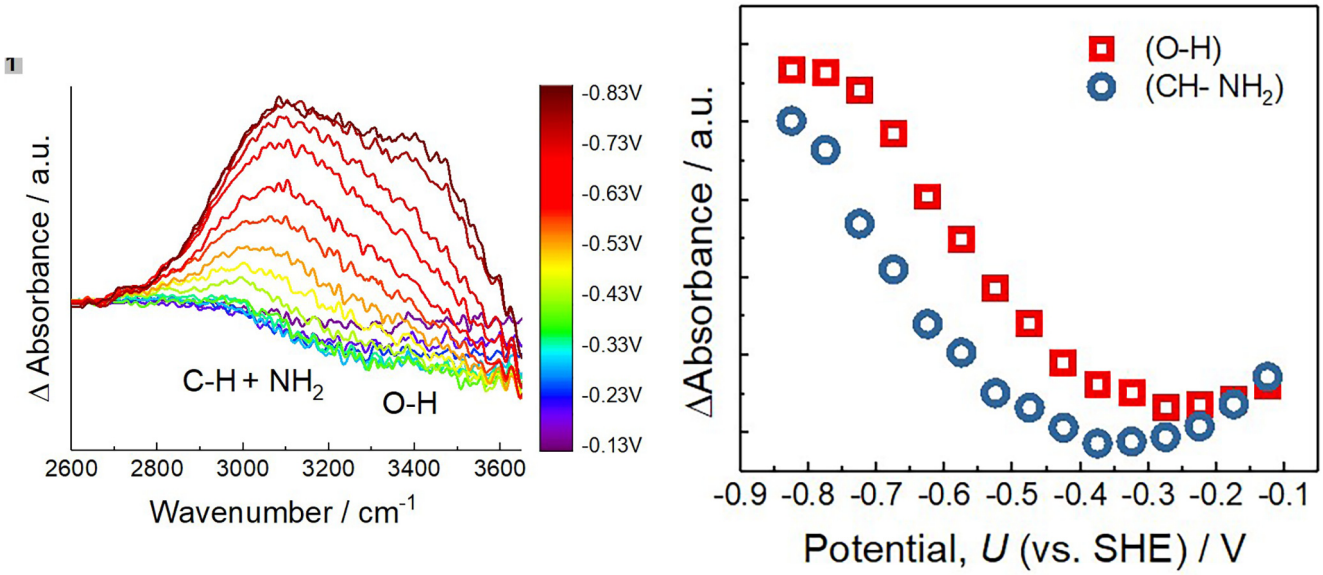

Fig. 5. *In-situ* FTIR investigation of Fe-P glycine electrolyte in the range of 2600–3600 cm^{-1}. Applied potential from −0.13 to −0.83 V vs. SHE. 0.7 M $FeSO_4$; 0.06 M $NaH_2PO_2 \cdot H_2O$; 0.21 M glycine.

Table 1
Vibrational frequencies of adsorbed glycine.

ν/cm^{-1}	Assignment	Reference
3600–3400	O-H stretching	[21,31]
3825–3200	CH_2 +NH_2 stretching	[21,31,32]
1602	asym. str. COO^- + bend NH^+_3	[4,21,28,31,32]
1500	bend NH_2	[4,21,32]
1446	bend CH_2	[31]
1412	sym. str. COO^- + bend NH_2	[4,21,28,32]
1331	wagging NH_3 + bend CH_2	[4,21,28,31,32]

of glycine, the Nyquist result shows inductive loops (Fig. 7) at potentials where Fe-P deposition took place ($U \leq -0.67$ V [35] i n publication). These results can successfully be interpreted by an equivalent electric circuit (EEC) shown at the Nyquist plot in Fig. 7. R1 is a series resistance mainly due to the solution. CPE1 is a constant phase element (CPE) representing the interfacial capacity. R2 is the charge transfer resistance. The partial circuit consisting of the resistance R3 and the inductance L1 model the influence of intermediates on charge transfer. Fitting of the experimental results by this equivalent circuit yielded the respective element values (Table 2). The effective values of the double layer capacitance (C_{eff}) were calculated according to Ref. [36].

$$C_{eff} = Y\left(f'' max\right)^{n-1} \quad (18)$$

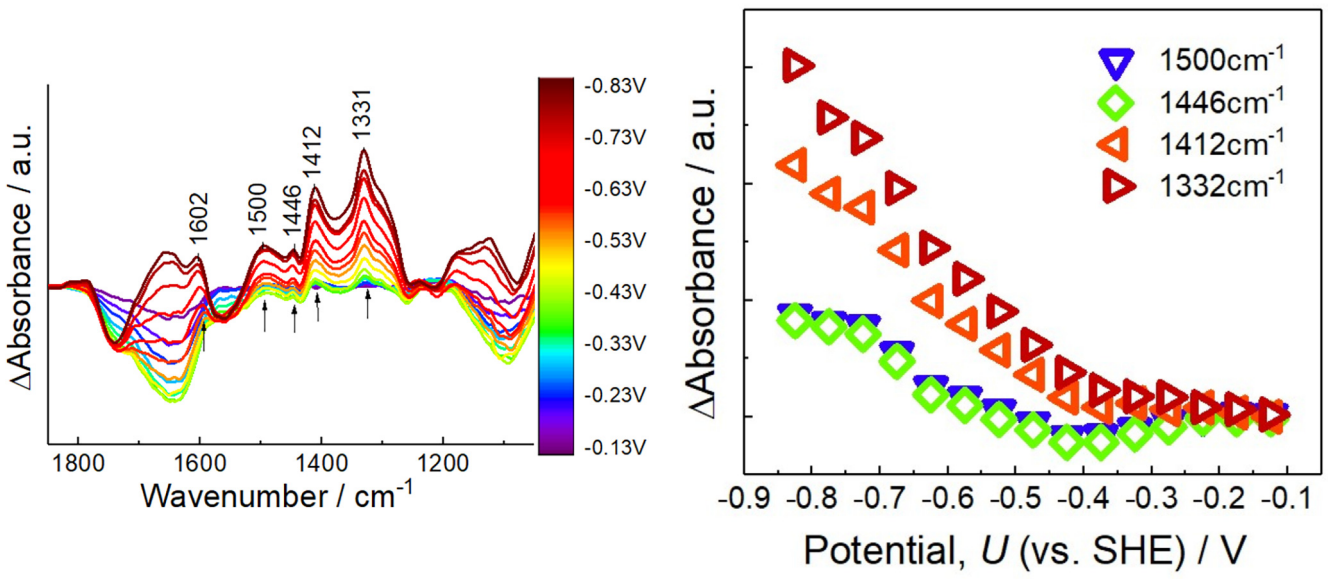

Fig. 6. *In-situ* FTIR investigation of Fe-P glycine electrolyte in range of 1000–1800 cm^{-1}. Applied potential from −0.13 to −0.83 V vs. SHE. 0.7 M $FeSO_4$; 0.06 M $NaH_2PO_2 \cdot H_2O$; 0.21 M glycine.

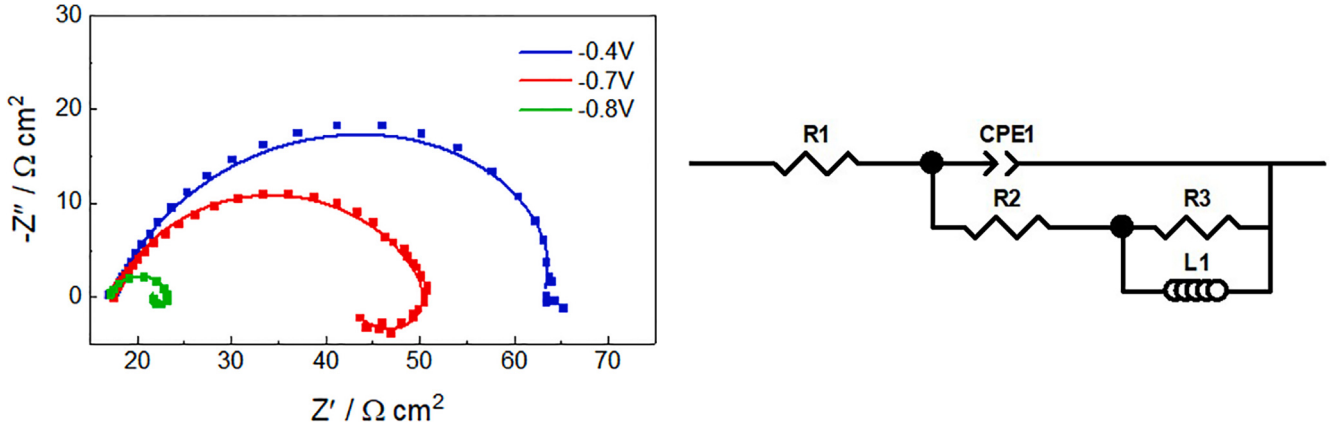

Fig. 7. Electrochemical impedance spectra (Nyquist plot). 0.7 M $FeSO_4$; 0.06 M $NaH_2PO_2 \cdot H_2O$; no glycine. Experimental data fitted to the indicated equivalent electric circuit. Electrode potentials (vs. SHE) indicated.

Table 2
Equivalent circuit parameters. Glycine-free solution (comp. Fig. 7).

Potential/V	R1/Ωcm^2	CPE1/Fs^{n-1}cm^{-2}	C_{eff}/μFcm^{-2}	n	R2/Ωcm^2	R3/Ωcm^2	L1/Hcm^2
−0.4	17.2	0.0091	7235.3	0.74	46.9	9.1	22.0
−0.7	17.4	0.00085	296.8	0.75	25.7	8.0	35.0
−0.8	16.8	0.0012	103.8	0.77	4.8	1.7	0.3

where (f''_{max}) represent the frequency at which the imaginary part of the impedance (Z''). Y is a parameter and n is the exponent of the constant phase element, respectively.

The constant phase element CPE1 is most probably determined by a distribution of active surface sites and by an inhomogeneity of the dielectric constant due to the variation in chemical composition of the Fe-P layer involving a number of intermediate adsorption stages [34, 37]. The inductive behaviour at low frequencies during Fe-P deposition ($U = -0.7$ and -0.8 V) was caused by differences of the intermediate adsorption rate and its subsequent reduction. When the number of intermediate adsorption steps increases, the impedance spectrum becomes more complicated [38].

C_{eff} at $U = -0.4$ V is comparably high (Table 2). It probably not only represents the double layer capacity (typically 10–40 μFcm^{-2}), but also is affected by the strong adsorption of intermediate Fe(I) compounds like e.g. $FeOH^+$. At more negative potentials, hydrogen evolution and a faster Fe-P deposition reaction facilitate the reduction of intermediates, so that C_{eff} attains more typical values for a double layer capacity. In parallel, the charge transfer resistance R2 decreases.

In the presence of glycine (Fig. 8), the Nyquist plots show only two semicircles without any induction loops. The impedance spectra obtained at $U = -0.4$ V, where only hydrogen is evolved, the electrode process is modelled by the EEC in Fig. 8a. It contains a circuit representing the adsorption of glycine with resistance R3 and the adsorption capacitance CPE2; R2 is again the faradaic

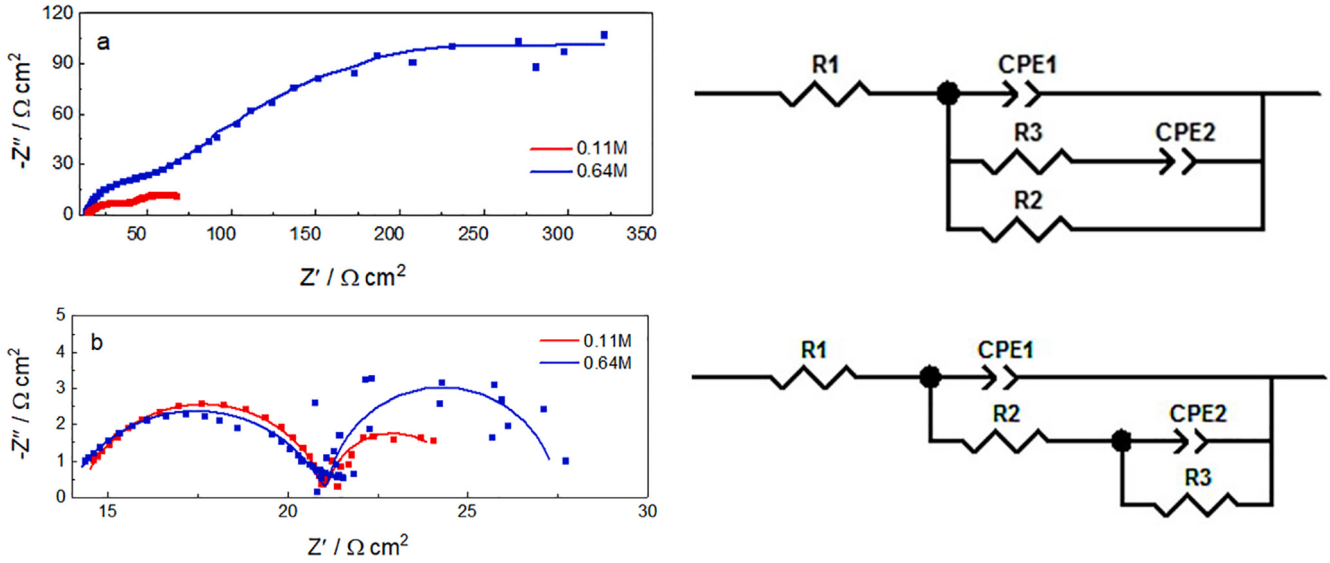

Fig. 8. Electrochemical impedance spectra (Nyquist plot). 0.7 M $FeSO_4$; 0.06 M $NaH_2PO_2 \cdot H_2O$; glycine concentrations indicated. Experimental data fitted to the indicated equivalent electric circuits. Electrode potentials vs. SHE (a) −0.4 V, (b) −0.8 V.

Table 3
Equivalent circuit parameters. Various glycine concentrations (comp. Fig. 8).

c[H(gly)]/M	Potential/V	R1/Ωcm^2	CPE1/Fs^{n-1}cm^{-2}	C_{eff1}/μFcm^{-2}	n	R2/Ωcm^2	CPE2/Fs^{n-1}cm^{-2}	C_{eff2}/μFcm^{-2}	n	R3/Ωcm^2
0.11	−0.4	13.6	0.002	65.8	0.54	57.5	0.0078	7699.8	0.69	66.6
0.64		13.2	0.000097	11.2	0.82	52.3	0.0016	1153.0	0.60	464.4
0.11	−0.8	14.2	0.00012	10.2	0.83	6.8	0.069	72530.2	1.02	3.5
0.64		4.7	0.00089	29.5	0.72	2.1	0.68	691524.4	0.96	2.4

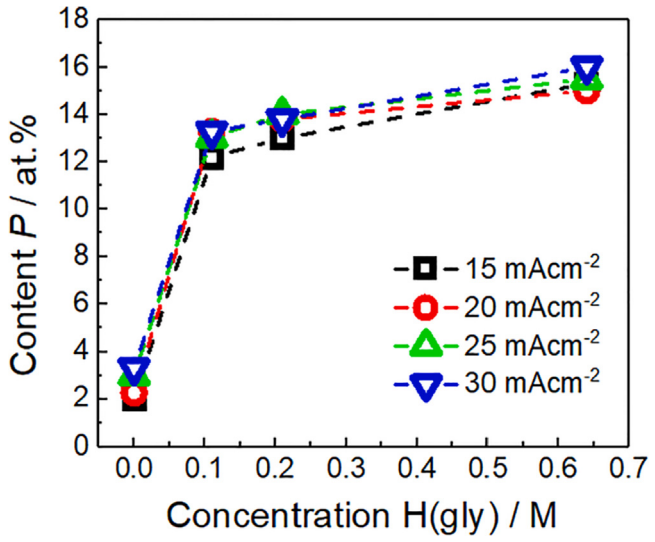

Fig. 9. Dependence of phosphorus content in Fe-P alloys on the glycine H(gly) concentration in the electrolyte at various current densities.

resistance of the hydrogen evolution (Table 3). In the presence of glycine, C_{eff1} is close to the expected double layer capacity. Because glycine enhances the hydrogen evolution, the pH increases locally and facilitates the reduction of adsorbed oxygen-containing intermediates such as $FeOH^+$.

At $U = -0.8$ V, where Fe-P electrodeposition occurred in the presence of glycine, two semicircles appeared in the Nyquist plot (Fig. 8b). The data were fitted to the EEC containing adsorbed intermediates (R3 and CPE2). The increase of the glycine concentration decreased the charge transfer resistance (R2) and decreased the adsorption impedance (circuit CPE2 and R3; Table 3), i.e. glycine adsorption facilitates the electrodeposition of Fe-P alloy.

3.5. Composition and morphology of Fe-P coatings

Analysis of the EDX data (Fig. 9) showed a dependency of the glycine concentration on the phosphorous content of the deposits obtained with various current densities (10, 20, 25, 30 mA/cm^2) applying the same charge (thickness ~10–12 μm). Glycine addition results in almost an order of magnitude increase in P content. Further glycine additions exhibit a moderate and steady P content increase.

The increasing glycine concentration leads to an increase of the $Fe(gly)^+$ species which causes a lower deposition rate of iron so that the hypophosphite reduction rate can increase:

$$H_3PO_2 + H^+ + e^- \rightleftharpoons P + 2H_2O \ (U^\circ = -0.508\ V) \quad (19)$$

and the phosphorous content in the deposit can increase. Even when dissolved oxygen in the electrolyte may lead to H_3PO_3, it may be re-reduced to H_3PO_2 almost at the same potential:

$$H_3PO_3 + 2H^+ + 2e^- \rightleftharpoons H_3PO_2 + H_2O \ (U^\circ = -0.499\ V). \quad (20)$$

The morphology of the deposits changes from microcrystalline (Fig. 10a) to nanocrystalline (Fig. 10b) upon addition of glycine [35,39]. XRD studies of Fe-P coatings showed the appearance of the broad bands at P concentrations higher than 13 at.% indicating amorphous morphologies [15,40]. According, to these studies the amorphous coatings can be deposited with glycine concentrations >0.2 M (comp. Fig. 9).

The appearance of the Fe-P deposit negative of about −0.75 V (Fig. 4) may be based on the formation of mainly two Fe complexes, either with hypophosphite (comp. Ref. [41]):

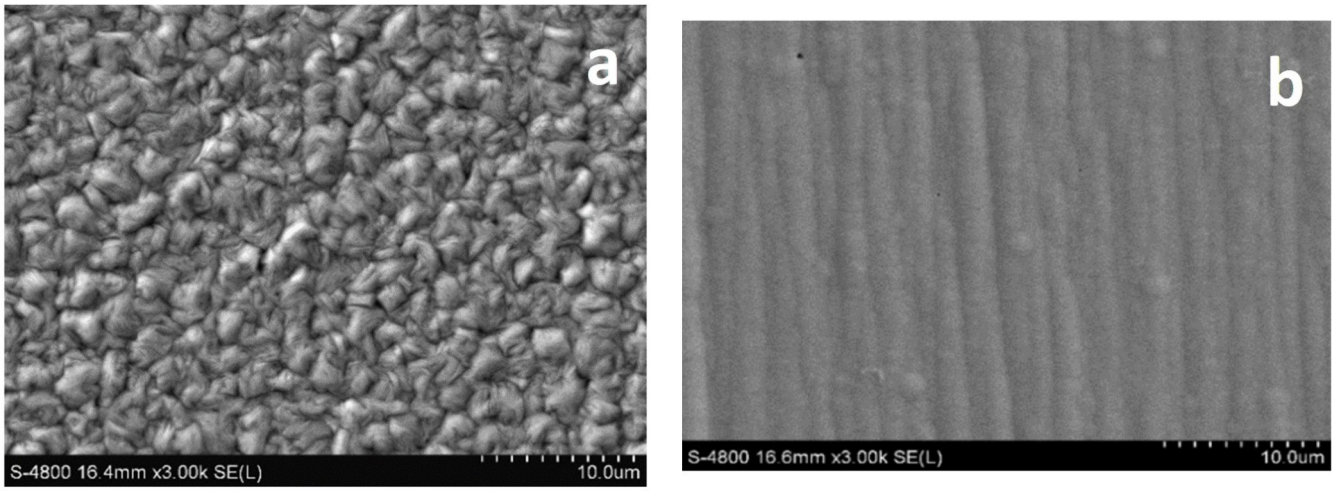

Fig. 10. SEM morphology of deposited Fe-P coatings electrodeposited (a) without glycine H(gly) and (b) with 0.21 M H(gly). Current density 30 mA/cm^2, 6 0 °C. P content: (a) 4 at.%; (b) 13 at.% (comp. Fig. 9).

$$Fe^{2+}{}_{aq} + H_2PO_2^- \rightarrow [Fe(H_2PO_2)]^+{}_{ads} \quad (21)$$

or the species $Fe(gly)^+{}_{ads}$ adsorbed on the negatively charged electrode surface which can be reduced to Fe according to Eq. (13).

4. Conclusions

A mechanistic investigation of the influence of glycine on the Fe-P electrodeposition was presented applying the Electrochemical Quartz Microbalance (EQMB), *in-situ* external reflection FTIR spectroscopy, and the Electrochemical Impedance Spectroscopy (EIS).

Hydrogen evolution sets in at potentials (vs. SHE) negative of ca. −0.40 V and Fe-P deposition at ca. −0.75 V. Due to a limited current efficiency of the Fe-P deposition, hydrogen evolution causes a pH increase near to the electrode surface. Therefore, the existence of adsorbed $H_2(gly)^+$, $H(gly)^{\pm}$ $Fe(gly)^+$ and the chelate complex $Fe(gly)_2$ in solution is suggested.

The extent of the Fe-P electrodeposition determined by charge and mass evaluations decreases strongly with the glycine concentration accompanied by an increase of hydrogen evolution. That means that the current efficiency of the Fe-P deposition drops with the glycine concentration. The hydrogen evolution rate is higher on Fe-P than on Au because the catalytic activity of Au is lower.

In-situ FTIR investigation showed an increase of glycine adsorption in the potential range of hydrogen evolution. This adsorption increase is retarded once Fe-P is deposited at potentials more negative than ca. −0.7 V. This is supported by EIS measurements.

The phosphorous content of the Fe-P deposit increases with the glycine concentration because the formation of the adsorbed $Fe(gly)^+$ species retards the deposition rate of iron relative to the hypophosphite reduction rate resulting in phosphorous.

Acknowledgment

Funding by the HORIZON2020 SELECTA Project (Nr. 642642), partial support by the HORIZON2020 Project SMARTELECTRODES (No. 778357), and by the Research Council of Lithuania (Project No. 09.3.3-LMT-K-712-08-0003) is acknowledged. The authors are grateful to Veronica Gman and Gabriela Sandulache (Hirtenberger Engineered Surfaces GmbH) for experimental assistance (SEM) and discussions.

References

[1] J.A. Davlatshoeva, G.B. Eshova, M.M. Rahimova, M.O. Guriev, L. V Kvyatkovskaya, Processes of formation of glycinate complexes of iron (II) and iron (III) under various ional forces of solution, Am. J. Chem. 7 (2) (2017) 58–65.
[2] M.H. Allahyarzadeh, M. Aliofkhazraei, A.R. Rezvanian, V. Torabinejad, A.R. Sabour Rouhaghdam, Ni-W electrodeposited coatings: characterization, properties and applications, Surf. Coating. Technol. 307 (2016) 978–1010.
[3] T. Yanai, T. Yamaguchi, T. Akiyoshi, K. Takashima, M. Nakano, H. Fukunaga, Effects of glycine in DES-based plating baths on structural and magnetic properties of Fe-Ni films, IEEE Trans. Magn. 53 (11) (2017) 1–4.
[4] R.A.J. Critelli, P.T.A. Sumodjo, M. Bertotti, R.M. Torresi, Influence of glycine on Co electrodeposition: IR spectroscopy and near-surface pH investigations, Electrochim. Acta 260 (2018) 762–771.
[5] W. Yin, L. Huang, E. Bjerglund, C. Frandsen, H. Christian, B. Hansen, Glycine buffered synthesis of layered iron (II) -iron (III) hydroxides (green rusts), J. Colloid Interface Sci. 497 (2017) 429–438.
[6] I. Saberikia, E. Safaei, M.H. Kowsari, Y.I. Lee, P. Cotic, A new iron(III) complex of glycine derivative of amine-chloro substituted phenol ligand: synthesis, characterization and catechol dioxygenase activity, J. Mol. Struct. 1029 (2012) 60–67.
[7] J. Guo, X. Guo, S. Wang, Z. Zhang, J. Dong, Effects of glycine and current density on the mechanism of electrodeposition, composition and properties of Ni-Mn films prepared in ionic liquid, Appl. Surf. Sci. 365 (2016) 31–37.
[8] M. Hrubovčakova, M. Kupkova, M. Džupon, Fe and Fe-P foam for biodegradable bone replacement material: morphology, corrosion behaviour, and mechanical properties,, Ann. Mater. Sci. Eng. 2016 (2016) 1–9.
[9] L. Huang, X.M. Zheng, Y.S. Wu, L.J. Xue, F.S. Ke, Electrodeposition and lithium storage performance of novel three-dimensional porous Fe-Sb-P amorphous alloy electrode, Electrochem. Commun. 11 (3) (2009) 585–588.
[10] X.M. Zheng, P.Y. Zhang, L.K. Wang, S. Tao, Y.X. Wang, J.T. Li, Superior Li storage anode based on novel Fe-Sn-P alloy prepared by electroplating, Electrochim. Acta 247 (2017) 314–320.
[11] S. Jafari, A. Beitollahi, B. Eftekhariyekta, K. Kanada, T. Ohkubo, G. Herzer, Microstructural and magnetic properties study of Fe-P rolled sheet alloys, J. Magn. Magn. Mater. 358 (2014) 38–43.
[12] S.K. Manna, D.B. Prabhu, R. Gopalan, V. Srinivas, "AC magnetic properties and core loss behavior of Fe–P soft magnetic sheets, IEEE Trans. Magn. 50 (11) (2014) 4–7.
[13] J. Herreros, F. Plazaola, Correlation between structure and magnetic behavior of Fe-P amorphous alloys, Phys. Rev. B 52 (17) (1995).
[14] A. Mikó, E. Kuzmann, M. Lakatos-Varsányi, A. Kákay, F. Nagy, L.K. Varga, Mössbauer and XRD study of pulse plated Fe-P and Fe-Ni thin layers, Hyperfine Interact. 165 (1–4) (2007) 195–201.
[15] M. Hong, D. Jin, J. Soo, "The effects of pH and temperature on Ni–Fe–P alloy electrodeposition from a sulfamate bath and the material properties of the deposits, Thin Solid Films 489 (2005) 122–129.
[16] C.A.C. Sequeira, D.M.F. Santos, P.S.D. Brito, Electrocatalytic activity of simple and modified Fe-P electrodeposits for hydrogen evolution from alkaline media, Energy 36 (2011) 847–853.
[17] M. Naka, K. Hashimito, T. Masumoto, Change in corrosion behavior of amorphous Fe-P-C alloys by alloying with various metallic elements, J. Non-Cryst. Solids 31 (1979) 355–365.
[18] J. Vatrál, R. Boča, W. Linert, Electrochemical investigation of the redox couple Fe(III)/Fe(II) in the presence of amino acids and neurotransmitters, Electrochim. Acta 145 (2014) 53–63.
[19] P. Vukosav, M. Mlakar, Speciation of biochemically important iron complexes with amino acids: L-aspartic acid and L-aspartic acid - Glycine mixture, Electrochim. Acta 139 (2014) 29–35.
[20] F. Safizadeh, N. Sorour, E. Ghali, G. Houlachi, Study of the hydrogen evolution reaction on Fe-Mo-P coatings as cathodes for chlorate production, Int. J. Hydrogen Energy 42 (8) (2016) 5455–5463.
[21] A.P. Sandoval, M. Orts, A. Rodes, J.M. Feliu, "Adsorption of Glycine on Au (hkl) and gold thin film Electrodes : an in situ spectroelectrochemical study, J. Phys. Chem. C 115 (2011) 16439–16450.
[22] D.T. Sawyer, A. Sobkowiak, Electrochemistry for Chemists, second ed., 1995. New York.
[23] C. Zafiu, G. Trettenhahn, D. Pum, U.B. Sleytr, W. Kautek, Structural control of surface layer proteins at electrified interfaces investigated by in situ Fourier transform infrared spectroscopy, Phys. Chem. Chem. Phys. 13 (29) (2011) 13232–13237.
[24] R.J. Martell, A.E., R.M. Smith, Motekaitis, "critically selected stability constants of metal complexes, NIST Stand. Ref. Database 46 (2004).
[25] R.J. Lemire, U. Berner, C. Musikas, D.A. Palmer, P. Taylor, O. Tochiyama, Chemical Thermodynamics of Iron Part 1, vol. 13a, 2013.
[26] S. Armyanov, S. Vitkova, O. Blajiev, Internal stress and magnetic properties of electrodeposited amorphous Fe-P alloys, J. Appl. Electrochem. 27 (1997) 185–191.
[27] E. McCafferty, Thermodynamics of Corrosion: Pourbaix Diagrams, first ed., Springer-Verlag, New York, 2010.
[28] D.C. Harris, Quantitative Chemical Analysis, seventh ed., 2007. New York.
[29] L. Chen, T. Uchida, H. Chang, M. Osawa, "Adsorption and oxidation of glycine on Au electrode : an in situ surface-enhanced infrared study, Electrochem. Commun. 34 (2013) 56–59.
[30] D.D. Bodé, T.N. Andersen, H. Eyring, Anion and pH effect on the potentials of zero charge of gold and silver electrodes, J. Phys. Chem. 71 (4) (1967) 792–797.
[31] I.T. Bae, D.A. Scherson, E.B. Yeager, Infrared spectroscopic determination of pH changes in diffusionally decoupled thin-layer electrochemical cells, Anal. Chem. 62 (1) (1990) 45–49.
[32] A.F. Gil, L. Salgado, L. Galicia, I. González, Predominance-zone diagrams of Fe(III) and Fe(II) sulfate complexes in acidic media. Voltammetric and spectrophotometric studies, Talanta 42 (3) (1994) 407–414.
[33] T. Rosado, M. Leonor, T.S. Duarte, R. Fausto, Vibrational spectra of acid and alkaline glycine salts, Vib. Spectrosc. 16 (1) (1998) 35–54.
[34] S.L. Díaz, J.A. Calderón, O.E. Barcia, O.R. Mattos, Electrodeposition of iron in sulphate solutions, Electrochim. Acta 53 (25) (2008) 7426–7435.
[35] N. Kovalska, et al., Electrodeposition of Nanocrystalline Fe-P Coatings: Influence of Bath Temperature and glycine Concentration on Their Structural Properties, Mechanical and Corrosion Behaviour, (In Publication), 2019. Coatings.
[36] C.H. Hsu, F. Mansfeld, "Technical note: concerning the conversion of the constant phase element parameter (Y0) into a Capacitance, Corrosion 57 (9) (2001) 747–748.
[37] N.V. Sotskaya, O.V. Dolgikh, Kinetics of cathodic reduction of hypophosphite anions in aqueous solutions, Russ. J. Electrochem. 41 (12) (2005) 1336–1340.
[38] A. Lasia, Electrochemical Impedance Spectroscopy and its Applications, vol. 32, Kluwer Academic/Plenum Publishers, New York, 1999.

[39] N. Kovalska, W.E.G. Hansal, N. Tsyntsaru, H. Cesiulis, A. Gebert, W. Kautek, “Electrodeposition and corrosion behaviour of nanocrystalline Fe—P coatings, Trans. IMF 97 (2) (2019) 89—94.
[40] S. Vitkova, M. Kjuchukova, G. Raichevski, Electrochemical preparation of amorphous Fe-P alloys, J. Appl. Electrochem. 18 (5) (1988) 673—678.
[41] P.L. Cavallotti, L. Magagnin, C. Cavallotti, Influence of added elements on autocatalytic chemical deposition electroless NiP, Electrochim. Acta 114 (2013) 805—812.